Microscopic approach to the response of ^{3}He-^{4}He mixtures

A. Fabrocini and L. Vichi
Department of Physics, University of Pisa, Istituto Nazionale di Fisica Nucleare, Sezione di Pisa, I-56100 Pisa, Italy

F. Mazzanti and A. Polls
Departament d'Estructura i Constituents de la Matèria, Universitat de Barcelona, Diagonal 647, E-08028 Barcelona, Spain

(Received 22 November 1995; revised manuscript received 17 June 1996)

Correlated-basis-function perturbation theory is used to evaluate the zero-temperature response $S(q,\omega)$ of ^{3}He-^{4}He mixtures for inelastic neutron scattering, at momentum transfers q ranging from 1.1 to 1.8 Å^{-1}. We adopt a Jastrow correlated ground state and a basis of correlated particle-hole and phonon states. We insert correlated one-particle–one-hole and one- and two-phonon states to compute the second-order response. The decay of the one-phonon states into two-phonon states is accounted for in the boson-boson approximation. The full response is split into three partial components $S_{\alpha\beta}(q,\omega)$, each of them showing a particle-hole bump and a one phonon, δ-shaped peak, which stays separated from the multiphonon background. The cross term $S_{34}(q,\omega)$ results to be of comparable importance to $S_{33}(q,\omega)$ in the particle-hole sector and to $S_{44}(q,\omega)$ in the phonon one. Once the response has been convoluted with the experimental broadening, the computed scattering function is in semiquantitative agreement with recent experimental measurements. [S0163-1829(96)07637-0]

I. INTRODUCTION

Isotopic atomic helium mixtures are an intriguing case for many-body physicists. There exists a large body of experimental data, concerning mostly static properties (for instance, the chemical potentials and the maximum solubility[1–3]). Excitation spectra and related quantities, as the zero concentration ($x_3=0$) ^{3}He effective mass (m_3^*), have been also measured.[4] Recently, inelastic neutron scattering experiments have been carried out both at low, or intermediate, and high momentum transfers.[6,7] In both regions the measured response presents two generally distinguishable structures, to be ascribed to bosonlike collective excitations (phonons and rotons) and to Fermi particle-hole ones. However, this apparently simple picture hides a large interplay between the components of the mixtures, each of them probably contributing on comparable foot to both branches of the response. The reason for this lies in the large correlation effects, which are present in the system because of the strong interatomic potential and of the large density. These are also the motivations why truly microscopic and *ab initio* studies of helium mixtures are difficult, and, in the case of the response, practically absent in literature.

Qualitative studies of the response have been done in Ref. 8 (using a matrix dispersion-relation representation), in Ref. 9 within a correlated random phase approximation (very similar, in spirit, to the phenomenological polarization potential method used in Ref. 10 and, lately, in Ref. 11) and in Ref. 12 with a sum rules approach. Here we will employ the correlated basis function[13] (CBF) perturbation theory, to embody the above correlation effects directly into the basis functions. CBF has shown to be a powerful tool to successfully study helium at zero temperature: the energetics of both pure ^{4}He and ^{3}He are well described by sophisticated correlated ground state wave functions, containing explicit two-, three-body, backflow and spin correlations;[14–16] properties of one ^{3}He impurity in ^{4}He, such as chemical potential and effective mass are also quantitatively reproduced by such correlated wave functions.[17] In particular, by using CBF based perturbation theory, with the insertion of up to two correlated independent phonon intermediate states, the impurity effective mass m_3^* turns out to be $2.2m_3$, to be compared with the experimentally measured $2.3m_3$ value.

The behavior of the ^{3}He effective mass with the concentration in dilute mixtures has been recently object of some debate. Specific heat measurements[18,19] at finite x_3 do not show appreciable deviations from its $x_3=0$ value. However, in Ref. 6 the authors have to postulate a much larger value ($m_3^*\sim 2.95m_3$ at $x_3=0.05$) in order to reproduce the position of the particle-hole response with a Lindhard-like function and using a simple Landau-Pomeranchuk (LP) quasiparticle spectrum,[20]

$$\epsilon_k(\mathrm{LP})=\epsilon_0+\frac{\hbar^2k^2}{2m_3^*}. \tag{1}$$

This contradiction does not appear if one modifies the LP spectrum (LP modified, or LPM) as

$$\epsilon_k(\mathrm{LPM})=\epsilon_0+\frac{\hbar^2k^2}{2m_3^*}\frac{1}{1+\gamma k^2}, \tag{2}$$

γ being a free parameter, whose experimentally estimated values[6] range from $\gamma\sim 0.08$ Å^2 to $\gamma\sim 0.13$ Å^2. There are both experimental[6,4] and theoretical[5] indications of a deviation from the simple LP form.

In a CBF based approach, we assume to have an homogeneous mixture of N_3 ^{3}He atoms and N_4 ^{4}He atoms in a volume Ω, with partial densities $\rho_{\alpha=3,4}=N_\alpha/\Omega$, total density $\rho=\rho_3+\rho_4$ and concentrations $x_\alpha=\rho_\alpha/\rho$. We will keep

constant densities, while letting N_α and the volume going to infinity. The nonrelativistic Hamiltonian of the mixture is

$$H=-\sum_{\alpha=3,4}\sum_{i=1}^{N_\alpha}\frac{\hbar^2}{2m_\alpha}\nabla_i^2+\frac{1}{2}\sum_{\alpha,\beta=3,4}\sum_{i\neq j}^{N_\alpha,N_\beta}V(r_{ij}), \quad (3)$$

where the interaction is the same for all the different pairs of the mixture.

A realistic, correlated, variational ground state wave function Ψ_0 is obtained by the Jastrow-Feenberg ansatz[21]

$$\Psi_0=F_J F_T F_{\rm BF}\phi_0(N_3), \quad (4)$$

where $\phi_0(N_3)$ is the ground state Fermi gas wave function for the ^{3}He component and F_J, F_T and $F_{\rm BF}$ are N-body correlation operators including explicit two-, three-body, and backflow dynamical correlations, respectively. Three-body correlations are important for a good description of the energetics both of the mixture[22] and of the impurity[17]. However, it is unlikely that they may strongly affect the dynamical response, as the static structure functions are little sensitive to their inclusion. Backflow correlations may play a more important role, but they show a complicate momentum dependence. This does not allow presently for a complete sum of the cluster diagrams containing this type of correlation, so increasing the uncertainty on the final result. For these reasons, we will limit our analysis to the case of two-body, state independent (or Jastrow) correlations only ($F_T=F_{\rm BF}=1$), but will include the effects of richer correlations by pushing forward the perturbative expansion in a Jastrow correlated basis.

F_J results to be

$$F_J(N_4,N_3)=\prod_{i_3<j_3}^{N_3}f^{(3,3)}(r_{i_3j_3})\prod_{i_4<j_4}^{N_4}f^{(4,4)}(r_{i_4j_4}) \times\prod_{i_3}^{N_3}\prod_{i_4}^{N_4}f^{(3,4)}(r_{i_3i_4}), \quad (5)$$

where $f^{(\alpha,\beta)}(r)$ are two-body correlation functions determined by minimizing the variational ground state energy.

It is possible to generate a correlated basis through the operator (5), to be used in a CBF perturbation theory (CBFPT). This theory has been successfully adopted for computing the inclusive response of nuclear matter and heavy nuclei to electron and hadron scattering[23–25], and has shown to be able to provide a semiquantitative agreement with experimental neutron inelastic scattering (nIS) data in pure, liquid atomic ^{4}He[26].

In this paper, we will apply CBFPT to compute the nIS response of the mixture, by considering as intermediate states the normalized, correlated ^{4}He n-phonon states (nPH) $|\mathbf{k}_1,\ldots,\mathbf{k}_n\rangle$, and ^{3}He n-particle, m-hole states (np-mh) $|\mathbf{p}_1,\ldots,\mathbf{p}_n,\mathbf{h}_1,\ldots,\mathbf{h}_m\rangle$.

The nPH states are given by

$$|\mathbf{k}_1,\ldots,\mathbf{k}_n\rangle =\frac{\rho_4(\mathbf{k}_1)\cdots\rho_4(\mathbf{k}_n)|\Psi_0\rangle}{\langle\Psi_0|\rho_4^\dagger(\mathbf{k}_n)\cdots\rho_4^\dagger(\mathbf{k}_1)\rho_4(\mathbf{k}_1)\cdots\rho_4(\mathbf{k}_n)|\Psi_0\rangle^{1/2}}, \quad (6)$$

where $\rho_4(\mathbf{k})$ is the ^{4}He density fluctuation operator

$$\rho_4(\mathbf{k})=\sum_{i=1,N_4}e^{i\mathbf{k}\cdot\mathbf{r_i}}. \quad (7)$$

Correlated np-mh states are obtained in a similar way, by applying the correlation operator to the Fermi gas excited states $\Phi_{\rm np-mh}(N_3)$,

$$|\mathbf{p}_1,\ldots,\mathbf{p}_n,\mathbf{h}_1,\ldots,\mathbf{h}_m\rangle=\frac{F_J|\Phi_{\rm np-mh}\rangle}{\langle\Phi_{\rm np-mh}|F_J^\dagger F_J|\Phi_{\rm np-mh}\rangle^{1/2}}. \quad (8)$$

We will consider one-phonon (1PH) and 1p-1h intermediate correlated states, which we will term as one intermediate excitation (OIE) states. The response computed at the OIE level will be called *variational*. In addition, we will also consider the possible decay of 1PH states into 2PH ones, which is essential in giving a physically meaningful ^{4}He excitation spectrum and provides a quenching of the one-phonon peak. This term will be computed in a boson-boson approximation, i.e., neglecting the ^{3}He antisymmetry. Such an approach may be justified on the basis of the low ^{3}He concentration.

1p-1h states may also be coupled to 1PH and 2PH. Such a coupling may be taken into account by a corresponding self-energy insertion. Its analogous in the problem of the single ^{3}He atom in ^{4}He is responsible for the impurity large effective mass. To estimate the importance of this effect we will use the on-shell part of the impurity self-energy, again relying on the small value of x_3.

The plan of the paper is as follows. In Sec. II we will briefly outline the CBFPT for the response of the mixture and the variational calculation will be described in some details. Section III is devoted to the description of the calculation of the coupling with the 2PH states and of the decays into 1PH and 2PH states. Section IV contains results for the response and the comparison with the experimental scattering functions. Moreover, the ^{4}He and ^{3}He excitation spectra are presented and discussed. Conclusions are drawn in Sec. V.

II. CBFPT FOR THE RESPONSE

The dynamical structure function (DSF) $S(q,\omega)$ of a ^{3}He-^{4}He mixture at $T=0$ is given by the imaginary part of the polarization propagator $D(q,\omega)$

$$S(q,\omega)=\frac{1}{\pi}{\rm Im}D(q,\omega), \quad (9)$$

where

$$D(q,\omega)=\frac{1}{N}\left\langle\tilde{\Psi}_0\left|\rho^\dagger(\mathbf{q})\frac{1}{H-E_0-\omega-i\eta}\rho(\mathbf{q})\right|\tilde{\Psi}_0\right\rangle, \quad (10)$$

and

$$\rho(\mathbf{q})=\rho_3(\mathbf{q})+\rho_4(\mathbf{q}), \quad (11)$$

$$\rho_\alpha(\mathbf{q})=\sum_{i=1,N_\alpha}e^{i\mathbf{q}\cdot\mathbf{r_i}} \quad (12)$$

and $N=N_3+N_4$. In Eq. (10), $\tilde{\Psi}_0$ is the exact ground state of H with eigenvalue E_0.

The total DSF may be expressed in terms of partial $\alpha\beta$ DSF, $S_{\alpha\beta}(q,\omega)$, as

$$S(q,\omega)=\sum_{\alpha,\beta=3,4} x_{\alpha\beta}S_{\alpha\beta}(q,\omega), \tag{13}$$

with $x_{\alpha\beta}=(x_\alpha x_\beta)^{1/2}$ and

$$S_{\alpha\beta}(q,\omega)=\frac{1}{\pi}\mathrm{Im}D_{\alpha\beta}(q,\omega)=\frac{1}{\pi}\mathrm{Im}\frac{1}{\sqrt{N_\alpha N_\beta}} \times\left\langle\tilde{\Psi}_0\middle|\rho_\alpha^\dagger(\mathbf{q})\frac{1}{H-E_0-\omega-i\eta}\rho_\beta(\mathbf{q})\middle|\tilde{\Psi}_0\right\rangle. \tag{14}$$

The experimentally measured nIS double differential cross section for the mixture directly provides access to the total scattering function $\hat{S}(q,\omega)$, which is in turn related to the partial DSF's by the relation

$$\hat{S}(q,\omega)=\frac{x_4\sigma_4S_{44}(q,\omega)+2x_{34}\sigma_{34}S_{34}(q,\omega)+x_3[\sigma_3S_{33}(q,\omega)+\sigma_3^iS_{33}^I(q,\omega)]}{x_4\sigma_4+x_3(\sigma_3^c+\sigma_3^i)}. \tag{15}$$

The elementary cross sections, as given by Sears[27] in units of barns, are $\sigma_4=1.34$, $\sigma_3=4.42$, $\sigma_3^i=1.19$, and $\sigma_{34}=2.35$. The spin-density DSF $S_{33}^I(q,\omega)$ also appears in the expression above, with the corresponding cross section σ_3^i. It describes ^{3}He spin fluctuations via the operator

$$\rho_3^{\mathbf{I}}(\mathbf{q})=\sum_{i=1,N_3} e^{i\mathbf{q}\cdot\mathbf{r}_i}\mathbf{I}_i, \tag{16}$$

where $\mathbf{I}_i$ is the spin of ^{3}He i nucleus.

We will focus, in the remainder, mainly on the calculation of $S_{\alpha\beta}$. To derive a perturbative expansion it is convenient to split H into an unperturbed piece H_0 and an interaction term H_1, as follows:

$$\langle m|H_0|n\rangle=\delta_{nm}\langle m|H|m\rangle=E_m^v, \tag{17}$$

and

$$\langle m|H_1|n\rangle=(1-\delta_{nm})\langle m|H|n\rangle=\tilde{H}_{mn}. \tag{18}$$

Here $|m\rangle$ are correlated basis states, eigenstates of H_0. In particular, $|0\rangle=|\Psi_0\rangle$ is not an eigenstate of H and its difference from $|\tilde{\Psi}_0\rangle$ is treated perturbatively. The expansion is obtained by writing

$$H-E_0=H_0-E_0^v+(H_1-\Delta E_0), \tag{19}$$

where ΔE_0 is the correction to the variational ground state energy E_0^v, and by developing the propagator $(H-E_0-\omega-i\eta)^{-1}$ in powers of $(H_1-\Delta E_0)$. A similar expansion is performed for the ground state $|\tilde{\Psi}_0\rangle$.

If the expansion is truncated at the lowest order, the partial DSF are given by

$$S_{\alpha\beta}(q,\omega)=\frac{1}{\sqrt{N_\alpha N_\beta}}\sum_n \langle\Psi_0|\rho_\alpha^\dagger(\mathbf{q})|n\rangle\langle n|\rho_\beta(\mathbf{q})|\Psi_0\rangle \times\delta(\omega-\omega_n), \tag{20}$$

with $\omega_n=E_n^v-E_0^v$.

As stated in the introduction, we will first consider only OIE insertions, i.e., correlated 1PH and 1p-1h intermediate states, defined as

$$|\mathbf{k}\rangle=\frac{\rho_4(\mathbf{k})|\Psi_0\rangle}{\langle\Psi_0|\rho_4^\dagger(\mathbf{k})\rho_4(\mathbf{k})|\Psi_0\rangle^{1/2}}, \tag{21}$$

$$|\mathbf{p},\mathbf{h}\rangle=\frac{F_J|\Phi_{1p-1h}\rangle}{\langle\Phi_{1p-1h}|F_J^\dagger F_J|\Phi_{1p-1h}\rangle^{1/2}}. \tag{22}$$

A. The variational responses

The variational response is given by the sum of two components,

$$S_{\alpha\beta}(q,\omega)=S_{\alpha\beta}^{1PH}(q,\omega)+S_{\alpha\beta}^{1p-1h}(q,\omega), \tag{23}$$

where $S_{\alpha\beta}^{1PH}(q,\omega)$ has a 1PH intermediate state

$$S_{\alpha\beta}^{1PH}(q,\omega)=\frac{1}{\sqrt{N_\alpha N_\beta}}\sum_k \langle\Psi_0|\rho_\alpha^\dagger(\mathbf{q})|\mathbf{k}\rangle\langle\mathbf{k}|\rho_\beta(\mathbf{q})|\Psi_0\rangle \times\delta(\omega-\omega_k), \tag{24}$$

and $S_{\alpha\beta}^{1p-1h}(q,\omega)$ has a 1p-1h intermediate state

$$S_{\alpha\beta}^{1p-1h}(q,\omega)=\frac{1}{\sqrt{N_\alpha N_\beta}}\sum_{p,h} \langle\Psi_0|\rho_\alpha^\dagger(\mathbf{q})|\mathbf{p},\mathbf{h}\rangle \times\langle\mathbf{p},\mathbf{h}|\rho_\beta(\mathbf{q})|\Psi_0\rangle\,\delta(\omega-\epsilon_p+\epsilon_h). \tag{25}$$

ω_k and ϵ_p-ϵ_h are the variational energies of the OIE states considered.

ω_k is given by

$$\omega_k=\frac{1}{N_4}\frac{\langle\mathbf{k}|H-E_0^v|\mathbf{k}\rangle}{\langle\mathbf{k}|\mathbf{k}\rangle}=\frac{\hbar^2k^2}{2m_4S_{44}(k)}, \tag{26}$$

and corresponds to the well known Feynman spectrum.[28] In Eq. (26), $S_{44}(k)$ is the variational estimate of the 44 component of the static structure function (SSF), $S_{\alpha\beta}(k)$, given by

$$S_{\alpha\beta}(k)=\frac{1}{\sqrt{N_\alpha N_\beta}}\frac{\langle\Psi_0|\rho^\dagger_\alpha(\mathbf{k})\rho_\beta(\mathbf{k})|\Psi_0\rangle}{\langle\Psi_0|\Psi_0\rangle}. \quad (27)$$

In a similar way, the single particle energy (SPE) $\epsilon_{x=p,h}$ is obtained by

$$\epsilon_x=\frac{\langle\mathbf{x}|H-E_0^v|\mathbf{x}\rangle}{\langle\mathbf{x}|\mathbf{x}\rangle}, \quad (28)$$

where $|\mathbf{x}\rangle$ is a particle or hole correlated state. We will discuss later the evaluation of ϵ_x.

By using the definition of the SSF given in Eq. (27), $\xi_\alpha(\mathbf{q};\mathbf{k})\equiv\langle\Psi_0|\rho^\dagger_\alpha(\mathbf{q})|\mathbf{k}\rangle$ is readily obtained as

$$\xi_\alpha(\mathbf{q};\mathbf{k})=\sqrt{N_\alpha}\frac{S_{\alpha4}(k)}{\sqrt{S_{44}(k)}}\delta_{\mathbf{k}-\mathbf{q}}, \quad (29)$$

giving, for $S^{1\mathrm{PH}}_{\alpha\beta}(q,\omega)$,

$$S^{1\mathrm{PH}}_{\alpha\beta}(q,\omega)=\sum_k\frac{S_{\alpha4}(k)S_{4\beta}(k)}{S_{44}(k)}\delta_{\mathbf{k}-\mathbf{q}}\delta(\omega-\omega_k). \quad (30)$$

The one-phonon contribution to the variational α-β responses shows a δ-like behavior, whose strength is $Z^v_{\alpha\beta}(k)=S_{\alpha4}(k)S_{\beta4}(k)/S_{44}(k)$, and it is located at the Feynman phonon energy. We notice that (i) $Z^v_{44}(k)=S_{44}(k)$ and that (ii) the 33 and 44 variational DSF are positive [$S_{44}(k)$ being positive], whereas this may not be true for the 34 DSF.

The expression for the particle-hole response $S^{1\mathrm{p}-1\mathrm{h}}_{\alpha\beta}(q,\omega)$ is more involved. A detailed description for a pure Fermi system (specifically, nuclear matter) can be found in Ref. 23 and references therein. On the basis of that formalism, the extension to a boson-fermion mixture is straightforward.

In CBF theory, the nondiagonal matrix elements $\xi_\alpha(\mathbf{q};\mathbf{p},\mathbf{h})=\langle\Psi_0|\rho^\dagger_\alpha(\mathbf{q})|\mathbf{p},\mathbf{h}\rangle$ are computed by a cluster expansion in Mayer-like diagrams, built up by dynamical correlations, $(f^{(\alpha,\beta)})^2-1$, and by statistical ones. Infinite classes of cluster terms are then summed by Fermi hypernetted chain[22] (FHNC) technique.

The ξ_α are explicitly given by

$$\xi_\alpha(\mathbf{q};\mathbf{p},\mathbf{h})=\delta_{\mathbf{q}-\mathbf{p}+\mathbf{h}}\frac{1}{\sqrt{D(p)D(h)}}(\tilde{h}_{dd,\alpha3}(q)+\delta_{\alpha3}[1+\tilde{h}_{ed,33}(q)]), \quad (31)$$

where

$$\tilde{h}_{xy,\alpha3}(q)=\rho_\alpha\int d^3r e^{i\mathbf{q}\cdot\mathbf{r}}[g_{xy,\alpha3}(r)-\delta_{xy,dd}], \quad (32)$$

with $(x,y)=(d,e)$ and $g_{xy,\alpha\beta}(r)$ are partial radial distribution functions (RDF). In fact, the total $\alpha\beta$-RDF, $g_{\alpha\beta}(r)$, giving the probability of finding a α-type particle 1 at a distance r_{12} from a β-type particle 2,

$$g_{\alpha\beta}(r_{12})=\frac{N_\alpha(N_\beta-\delta_{\alpha\beta})}{\rho_\alpha\rho_\beta}\frac{\int d^3r_3\cdots d^3r_N|\Psi_0|^2}{\int d^3r_1\cdots d^3r_N|\Psi_0|^2}, \quad (33)$$

is computed in FHNC,[22] using the correlated g.s. Ψ_0 and it turns out to be written as

$$g_{\alpha\beta}(r_{12})=g_{dd,\alpha\beta}(r_{12})+\delta_{\beta3}g_{de,\alpha3}(r_{12})+\delta_{\alpha3}g_{ed,3\beta}(r_{12})+\delta_{\alpha3}\delta_{\beta3}g_{ee,33}(r_{12}). \quad (34)$$

The partial RDF are classified according to whether the external particle (1 or 2) is reached by a statistical correlation (i.e., if the particle is involved in an exchange loop, e-vertex), or by a dynamical correlation only (d vertex). The definitions of the partial RDF, together with the full set of the related FHNC equations, may be found in Ref. 22

Actually, Eq. (31) sums all cluster diagrams factorizable in products of *dressed* two-body diagrams, as discussed in Ref. 23. Nonfactorizable diagrams involving three particles are also taken into account, even if they do not appear in Eq. (31). However, they have been inserted, following Ref. 23.

The function $D(x=p,h)$ is

$$D(x)=1-\rho_3\int d^3r e^{i\mathbf{x}\cdot\mathbf{r}}(g_{dd,33}(r)-1)L(k_Fr), \quad (35)$$

where $L(k_Fr)$ is the FHNC generalization of the exchange Slater function $l(k_Fr)=3j_1(k_Fr)/(k_Fr)^3$, and k_F is the ^{3}He Fermi momentum ($k_F^3=3\pi^2\rho_3$).

Again, as $D(x)$ turns out to be positive, $S^{1\mathrm{p}-1\mathrm{h}}_{33,44}(q,\omega)$ are positive, whereas $S^{1\mathrm{p}-1\mathrm{h}}_{34}(q,\omega)$ may be not.

Finally, the spin fluctuation matrix element, $\xi^{\mathbf{I}}_3(\mathbf{q};\mathbf{p},\mathbf{h})=\langle\Psi_0|\rho^{\mathbf{I}\dagger}_3(\mathbf{q})|\mathbf{p},\mathbf{h}\rangle$, is simply given by

$$\xi^{\mathbf{I}}_3(\mathbf{q};\mathbf{p},\mathbf{h})=\delta_{\mathbf{q}-\mathbf{p}+\mathbf{h}}\frac{1}{\sqrt{D(p)D(h)}}. \quad (36)$$

III. CORRELATED ONE- AND TWO-PHONON INTERMEDIATE STATES

In this section we will first study the effect on the phonon responses of the insertion of orthogonal, correlated 2PH states:

$$|\mathbf{k}_1\mathbf{k}_2\rangle_o=(1-|\mathbf{k}\rangle\langle\mathbf{k}|)|\mathbf{k}_1\mathbf{k}_2\rangle, \quad (37)$$

where the 2PH states of Eq. (6) have been orthogonalized to the 1PH ones by a Gram-Schmidt procedure.

2PH states influence the partial polarization propagators $D_{\alpha\beta}(q,\omega)$ via the direct coupling to the ground state and via the decay of 1PH states into 2PH. The coupling to the g.s goes through the matrix element of the ^{3}He fluctuation operator,

$$\xi_3(\mathbf{q};\mathbf{k}_1,\mathbf{k}_2)=\langle\Psi_0|\rho^\dagger_3(\mathbf{q})|\mathbf{k}_1,\mathbf{k}_2\rangle_o, \quad (38)$$

[notice that $\xi_4(\mathbf{q};\mathbf{k}_1,\mathbf{k}_2)$ vanishes because of the Schmidt orthogonalization of the 2PH states], whereas the decay is driven by the nondiagonal matrix element of the Hamiltonian

$$a(\mathbf{k};\mathbf{k}_1,\mathbf{k}_2)=\langle\mathbf{k}|H_1|\mathbf{k}_1,\mathbf{k}_2\rangle_o. \quad (39)$$

These CBF matrix elements have been computed in a boson-boson approximation (treating the ^{3}He as a mass-3 boson) and by adopting the convolution approximation[21] (CA) for the three-body distribution functions. expansion

Their explicit expressions are

$$\xi_3(\mathbf{q};\mathbf{k}_1,\mathbf{k}_2)=\frac{S_{34}(k_1)S_{34}(k_2)}{\sqrt{S_{44}(k_1)S_{44}(k_2)}}\left(S_{33}(q)-\frac{S_{34}^2(q)}{S_{44}(q)}\right), \tag{40}$$

and

$$a(\mathbf{k};\mathbf{k}_1,\mathbf{k}_2) = \frac{\hbar^2}{\sqrt{N_4}2m_4} \times\left(\frac{\mathbf{k}\cdot\mathbf{k}_1 S_{44}(k_2)+\mathbf{k}\cdot\mathbf{k}_2 S_{44}(k_1)-k^2 S_{44}(k_1)S_{44}(k_2)}{\sqrt{S_{44}(k)S_{44}(k_1)S_{44}(k_2)}} - \sqrt{\frac{x_4}{x_3}}\frac{k^2 S_{34}(k)S_{34}(k_1)S_{34}(k_2)}{S_{44}(k)\sqrt{S_{44}(k)S_{44}(k_1)S_{44}(k_2)}}\right). \tag{41}$$

It is convenient, at this point, to introduce the correlated self-energy

$$\Sigma_1(k,\omega)=\frac{1}{2}\sum_{\mathbf{k}_1,\mathbf{k}_2}\frac{|a(\mathbf{k};\mathbf{k}_1,\mathbf{k}_2)|^2}{\omega_{k_1}+\omega_{k_2}-\omega-i\eta}, \tag{42}$$

and the function $\chi(\mathbf{q};k,\omega)$ given by

$$\chi(\mathbf{q};k,\omega)=\frac{1}{2}\frac{1}{\sqrt{N_3}}\sum_{\mathbf{k}_1,\mathbf{k}_2}a(\mathbf{k};\mathbf{k}_1,\mathbf{k}_2) \times\frac{1}{\omega_{k_1}+\omega_{k_2}-\omega-i\eta}\xi_3^{\dagger}(\mathbf{q};\mathbf{k}_1,\mathbf{k}_2). \tag{43}$$

If we define the dressed phonon propagator $G^d(k,\omega)$ as

$$G^d(k,\omega)=\frac{1}{\omega_k-\Sigma_1(k,\omega)-\omega-i\eta}, \tag{44}$$

then the phonon contributions to the polarization propagators can be rearranged as

$$D_{44}^{\mathrm{PH}}(q,\omega)=\frac{1}{N_4}\sum_{\mathbf{k}}|\langle\Psi_0|\rho_4^{\dagger}(\mathbf{q})|\mathbf{k}\rangle|^2 G^d(k,\omega), \tag{45}$$

$$D_{43}^{\mathrm{PH}}(q,\omega)=\frac{1}{\sqrt{N_3N_4}}\sum_{\mathbf{k}}\langle\Psi_0|\rho_4^{\dagger}(\mathbf{q})|\mathbf{k}\rangle G^d(k,\omega) \times\left[\langle\mathbf{k}|\rho_3(\mathbf{q})|\Psi_0\rangle+\frac{1}{\sqrt{N_4}}\chi(\mathbf{q};k,\omega)\right], \tag{46}$$

$$D_{33}^{\mathrm{PH}}(q,\omega)=\frac{1}{N_3}\sum_{\mathbf{k}}G^d(k,\omega)\left[\langle\mathbf{k}|\rho_3(\mathbf{q})|\Psi_0\rangle+\frac{1}{\sqrt{N_3}}\chi(\mathbf{q};k,\omega)\right]^2 +\frac{1}{2}\frac{1}{N_3}\sum_{\mathbf{k}_1,\mathbf{k}_2}\frac{|\langle\Psi_0|\rho_3^{\dagger}(\mathbf{q})|\mathbf{k}_1,\mathbf{k}_2\rangle_o|^2}{\omega_{k_1}+\omega_{k_2}-\omega-i\eta}. \tag{47}$$

The DSF are then obtained by taking the imaginary parts of $D_{\alpha\beta}$.

The relevant changes introduced by the insertion of the 2PH states in the phonon responses are (1) the strengths of the deltalike 1PH peaks $Z_{\alpha\beta}$ are generally quenched respect to $Z_{\alpha\beta}^{v}$ In the 44 case, we have

$$Z_{44}(k)=Z_{44}^{v}(k)\left(1+\frac{\partial\mathrm{Re}\Sigma_1(k,\omega)}{\partial\omega}\right)^{-1}_{\omega=\omega_k}. \tag{48}$$

Analogous corrections occur for $Z_{34}(k)$ and $Z_{33}(k)$, which are also affected by those parts of the polarization propagators containing $\xi_3(\mathbf{q};\mathbf{k}_1,\mathbf{k}_2)$; (2) the 1PH peaks are shifted by the real part of the on-shell self energy, since the ^{4}He spectrum is modified as

$$\omega_k\rightarrow\omega_k^{\mathrm{CBF}}=\omega_k+\mathrm{Re}\Sigma_1(k,\omega_k^{\mathrm{CBF}}); \tag{49}$$

(3) a multiphonon tail appears at large ω values, beyond the position of the 1PH peak, at the momentum transfers here considered.

IV. CBF RESPONSES

In the class of the Jastrow correlated wave functions, the best variational choice is provided by the solution of the Euler equations

$$0=\frac{\delta\langle\Psi_0|H|\Psi_0\rangle}{\delta f^{(\alpha\beta)}}. \tag{50}$$

The resulting equations have been derived, within the FHNC framework, and solved for the ^{3}He impurity problem,[29,30] for the boson-boson mixture[31] and, lately, for the real fermion-boson case.[9]

Another, often used approach consists in parametrizing the correlation functions and in minimizing the ground state energy with respect to the parameters. This is the choice we have adopted here. Besides that, some of the results we will present have been obtained within the average correlation approximation (ACA).[32] In ACA, the correlation functions are the same for all the types of pairs ($f^{(3,3)}=f^{(3,4)}=f^{(4,4)}$) and the differences in the distribution functions (or in the static structure functions) are due only to the different isotope densities and statistics. We will also show that going beyond the ACA does not significantly affect our results.

We have used three types of correlation functions: the time honored, short ranged McMillan form (SR) and two long ranged functions (LR and LR1).

The McMillan correlation, in ACA, is given by

$$f_{\mathrm{SR}}(r)=\exp\left[-\left(\frac{b\sigma}{r}\right)^5\frac{1}{2}\right], \tag{51}$$

where $b=1.18$ and $\sigma=2.556$ Å. The SR correlation function gives a good description of the short range behavior of the pair wave function but fails to reproduce long range properties. For instance, it does not ensure the linear behavior of the ^{4}He SSF at $k\rightarrow 0$ (the phonon dispersion). Such a dispersion reflects in a long range behavior of the correlation of the type $f(r\rightarrow\infty)-1\propto -r^{-2}$. To this aim, we have also used a modified form, having the correct long range structure (LR), given by

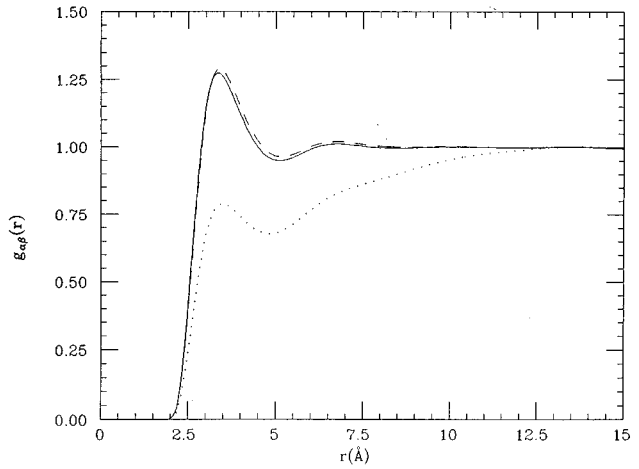

FIG. 1. Radial distribution functions for the mixture (see text). The solid line gives g_{44}, the dashed line g_{34}, and the dotted one is g_{33}.

$$f_{\mathrm{LR}}(r)=f_{\mathrm{SR}}(r)\left[A+B\exp\left(-\frac{(r-D)^2}{\tau r^4}\right)\right]. \qquad (52)$$

The parameters of $f_{\mathrm{LR}}(r)$, giving the variational minimum of the ^{4}He energy at the equilibrium density $\rho_0=0.02185$ Å^{-3}, are $b=1.18$, $A=0.85$, $B=1-A$, $D=3.8$ Å, and $\tau=0.043$ Å^{-2}. The B and τ parameters are related to the experimental pure ^{4}He sound velocity c and to the low-k behavior of its SSF by the relations

$$\frac{B}{\tau}=\frac{m_4 c}{2\pi^2\hbar\rho_0}; \quad S^{(4,4)}(k\to 0)=\frac{\hbar k}{2m_4 c}. \qquad (53)$$

In order to check the accuracy of ACA, we have also used a LR correlation (LR1), formally identical to f_{LR}, but with parameters depending on the type of the correlated pair. The 44 correlation function is the same as above, whereas the parameters of the 43 and 33 ones have been obtained by minimizing the energy of the pure ^{4}He with one and two ^{3}He impurities, respectively.

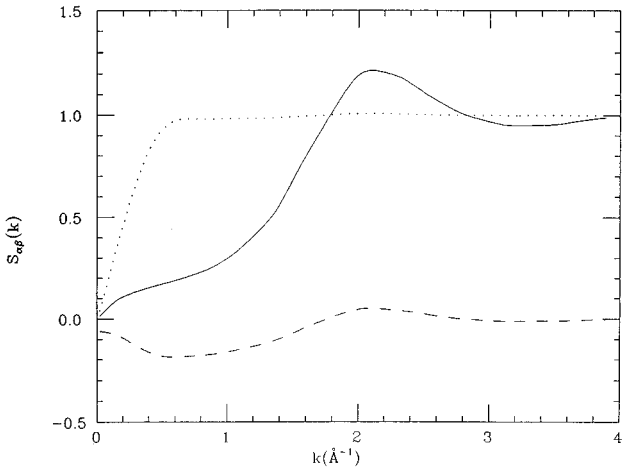

FIG. 2. Static structure functions for the mixture (see text). The solid line gives S_{44}, the dashed line S_{34}, and the dotted one is S_{33}.

TABLE I. Variational strengths and positions of the one phonon DSF responses with different correlations (see text). q in Å^{-1} and ω_q in K.

	q	ω_q	Z^v_{44}	Z^v_{34}	Z^v_{33}
SR	1.1	20.44	0.356	−0.146	0.060
LR		20.77	0.361	−0.145	0.058
LR1		20.75	0.362	−0.147	0.060
SR	1.3	20.74	0.491	−0.115	0.027
LR		21.68	0.461	−0.122	0.032
LR1		21.71	0.460	−0.122	0.032
SR	1.5	19.91	0.681	−0.072	0.008
LR		19.99	0.686	−0.071	0.007
LR1		20.02	0.685	−0.069	0.007
SR	1.7	19.20	0.908	−0.021	0.000
LR		19.24	0.899	−0.023	0.001
LR1		19.26	0.899	−0.019	0.000

Key ingredients in the CBF theory of the response in helium mixtures are the radial distribution functions $g_{\alpha\beta}(r)$ and the static structure functions $S_{\alpha\beta}(k)$. Figures 1 and 2 show these quantities in a 4.7% mixture, at a total density $\rho=0.02160$ Å^{-3}, for the $f_{\mathrm{LR1}}(r)$ correlation, in FHNC/0 approximation (i.e., we have neglected the elementary diagrams[22]). The results for the SSF, with the $f_{\mathrm{SR}}(r)$, differ mainly in the region of low-k values, in agreement with the previous discussion.

Table I shows the variational strengths $Z^v_{\alpha\beta}(k)$ of the one-phonon response for the same mixture and compares the results obtained with the SR and LR correlation functions at four momentum values, from $q=1.1$ to 1.7 Å^{-1}. The positions of the variational δ peaks, ω_k, are also given. It has to be noticed that the Feynman spectrum overestimates the experimental data by at least 10 K both in the maxon and roton regions. Table II provides the same quantities after the insertion of the 2PH states. $Z_{44}(k)$ of pure ^{4}He has been extensively and accurately studied in CBF in Ref. 26. Our approach, when applied to this system, gives similar results. As a matter of fact, at $k=2$ Å^{-1} (where its peak approximately

TABLE II. CBF strengths and positions of the one phonon DSF responses with different correlations (see text). q in Å^{-1} and ω_q in K.

	q	ω_q	Z_{44}	Z_{34}	Z_{33}
SR	1.1	13.73	0.275	−0.066	0.016
LR		13.69	0.272	−0.068	0.017
LR1		13.66	0.272	−0.068	0.017
SR	1.3	14.01	0.390	−0.045	0.005
LR		14.27	0.367	−0.047	0.006
LR1		14.25	0.366	−0.044	0.005
SR	1.5	13.84	0.559	−0.014	0.000
LR		13.79	0.558	−0.014	0.000
LR1		13.83	0.557	−0.011	0.000
SR	1.7	13.94	0.766	0.024	0.001
LR		13.94	0.766	0.024	0.001
LR1		13.96	0.765	0.027	0.001

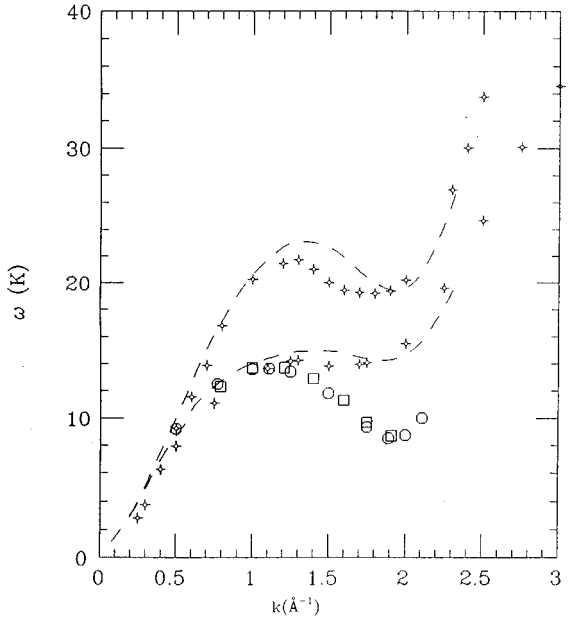

FIG. 3. ^{4}He excitation spectrum in the mixture (crosses) and in the pure system (dashed line). The upper curves are the Feynman spectra. Squares and circles are mixture experimental data (See text).

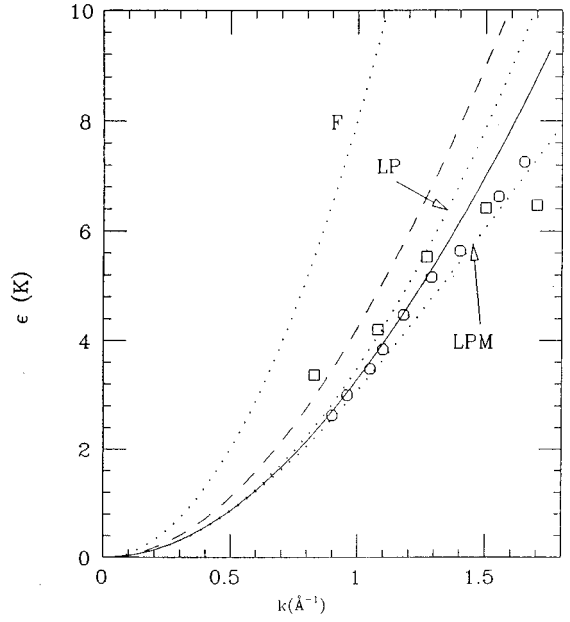

FIG. 4. ^{3}He single particle energies. The dashed line gives $\epsilon_k^{\rm CBF}$(CA), the solid line is $\epsilon_k^{\rm CBF}$ also shown are the LP, LPM, and free (F) energies. Squares and circles are the experimental data (See text).

lies) we obtain $Z_{44}^{\rm CBF}(k)=1.04$, vs $Z_{44}^{\rm expt}(k)=0.94$.[33] We have been able to push forward the CBF perturbative expansion in such a system, obtaining $Z_{44}^{\rm CBF}(k=2\ \text{Å}^{-1})=0.96$. As a further remark, we add that the use of either short or long range correlations little affects the strengths in the momentum region we have considered. This is also true for the other quantities that have been studied in this work.

Figure 3 shows the ^{4}He spectrum with the LR1 correlation. The figure also compares the spectrum with pure ^{4}He at ρ_0 and with the experimental results of Ref. 6 (circles) in a $x_3=1.1\%$ mixture at SVP and of Ref. 4 (squares) for a $x_3=6.0\%$ mixture.

The changes in going from pure ^{4}He to the mixture are clearly visible. These changes are mainly due to the lower ^{4}He density in the mixture and not to differences in the correlations. In fact, we obtain similar results if the LR-ACA correlation is used. CBF perturbative corrections appear to be large and bring the maxon energy close to the experiments. The roton is not well described, as it is too shallow respect to the data. This feature is also present in the ^{4}He case. We believe that most of the discrepancy in this part of the spectrum has to be ascribed to the use of CA in the calculation of the CBF matrix elements. Moreover, contributions from higher order CBF perturbative diagrams are known to be important to correctly reproduce the roton minimum in pure ^{4}He.[34] However, the CA results show a change in the sign of the shift from mixture to pure system at $q\simeq 1.8$ Å^{-1}, in good agreement with the measured experimental value[6] at constant pressure ($q\simeq 1.9$ Å^{-1}).

The boundaries of the 1p-1h DSF's are related to the energies of the 1p-1h state ϵ_p-ϵ_h. The variational SPE, $\epsilon_{p(h)}$, has been computed by the procedure of Ref. 35. However, because of the low ^{3}He density, it turns out to be extremely close to the free Fermi gas SPE,

$$\epsilon_k^{\rm FG}=\frac{\hbar^2k^2}{2m_3}. \tag{54}$$

Perturbative corrections to ϵ_k may be computed in CBF. In the case of the ^{3}He impurity, CBFPT provides an accurate evaluation of its SPE,[17,36] if the decay of the impurity excited state (given by a correlated plane wave) into correlated 1PH and 2PH states is considered. 1PH states account for $\sim 2/3$ of the difference between the experimental effective mass and the bare one, whereas 2PH states give the remainder. Because of the low density of the ^{3}He component, it is reasonable to expect a similar behavior in the finite concentration mixture. It implies that we should insert in the CBFPT expansion the coupling between 1p-1h states and 1PH and 2PH ones $[1\text{p}(1\text{h})\rightarrow 1\text{p}'(1\text{h}')+1(2)\text{PH}]$.

Work along this line is in progress. Here we have used for $\epsilon_k^{\rm CBF}$ the CBFPT SPE of the single impurity, obtained by extending to finite momenta the approach of Ref. 17 for the effective mass. The involved matrix elements have been computed in CA for the three-body distribution functions. CA gives $m_3^*({\rm CA})\sim 1.8m_3$ for the impurity, whereas the more realistic superposition approximation (SA) gives $m_3^*({\rm SA})\sim 2.2m_3$. However, the SA $k\neq 0$ matrix elements are much more involved than their CA counterparts, and their evaluation, together with a description of the method, will be presented subsequently.[36] Here, the effect of the missing effective mass has been estimated by simply scaling the CA SPE as $\epsilon_k^{\rm CBF}=[m_3^*({\rm CA})/m_3^*({\rm expt})]\epsilon_k^{\rm CBF}({\rm CA})$.

Figure 4 shows the ^{3}He impurity SPE in different approximations, and compares them with the experimental data (circles from Ref. 6 and squares from Ref. 4) and with the LP and LPM parametrizations given in the introduction, with parameters $m_3^*=2.3m_3$ and $\gamma=0.132$ Å^2. Even from the CA

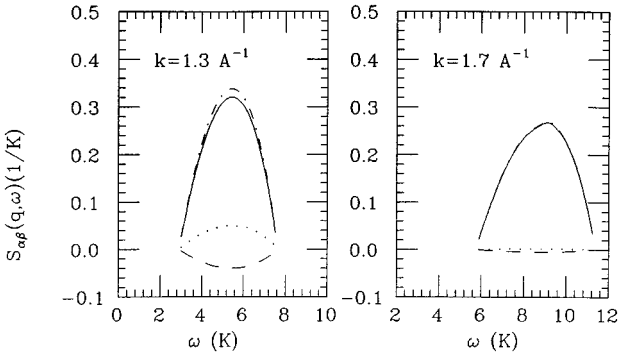

FIG. 5. 1p-1h DSF at $q=1.3$ and 1.7 Å^{-1}. The continuous line gives S_{33}, the dot-dashed S_{33}^{I} the dotted $10\times S_{44}$ and the dashed S_{34}.

calculation, a deviation from the LP behavior clearly appears. The estimated CBF value of γ in CA turns out to be $\gamma(\mathrm{CA})=0.052$ Å^2. We stress that, as for ^{4}He, we expect SA to provide a better description of the ^{3}He SPE behavior, as it correctly takes into account the core property of the system, requiring that the three-particle distribution functions vanish when any interparticle distance is lower than the radius of the repulsive core of the potential.

Figure 5 gives the 1p-1h DSF $S_{\alpha\beta}^{1\mathrm{p}-1\mathrm{h}}(q,\omega)$ at two momentum values ($q=1.3$ and 1.7 Å^{-1}), with the LR1 correlation and using $\epsilon_k^{\mathrm{CBF}}$ The two 33 DSF are very close and dominant, becoming indistinguishable at higher momenta; the 44 component is always very small (notice that it has been amplified by a factor of 10 in the figure); the 34 part is negative and an order of magnitude larger than $S_{44}^{1\mathrm{p}-1\mathrm{h}}$ in absolute value, contributing to decrease the total response mainly at low momenta. The free Fermi Gas DSF would be located to a larger energy with a lower peak strength, compatible with the fact that the correlated system has a ^{3}He effective mass 2.3 times larger than the bare mass (at $q=1.3$ Å^{-1} the FG peak position is $\omega=13.6$ K and the strength is $S_{33}^{1\mathrm{p}-1\mathrm{h}}(\mathrm{FG})=0.115$ K^{-1}). In addition, as for the phonon DSF, the use of the SR and LR correlations does not alter appreciably the results shown in the figure.

To evaluate the total scattering function $\hat{S}(q,\omega)$, the DSF must be multiplied by the elementary cross sections and the concentrations of the species. In Figs. 6(a) and 6(b) we give the partial CBF scattering functions (PSF):

$$\hat{S}_{44}(q,\omega)=\frac{x_4\sigma_4}{x_4\sigma_4+x_3(\sigma_3^c+\sigma_3^i)}S_{44}(q,\omega), \tag{55}$$

$$\hat{S}_{34}(q,\omega)=\frac{2x_{34}\sigma_{34}}{x_4\sigma_4+x_3(\sigma_3^c+\sigma_3^i)}S_{34}(q,\omega) \tag{56}$$

and

$$\hat{S}_{33}(q,\omega)=\frac{x_3}{x_4\sigma_4+x_3(\sigma_3^c+\sigma_3^i)}[\sigma_3 S_{33}(q,\omega)+\sigma_3^i S_{33}^{I}(q,\omega)]. \tag{57}$$

The LR1 correlation has been used. The position and the strength of the phonon contribution to the PSF's are explicitly given. In the 1p-1h sector, at the lower momentum, the

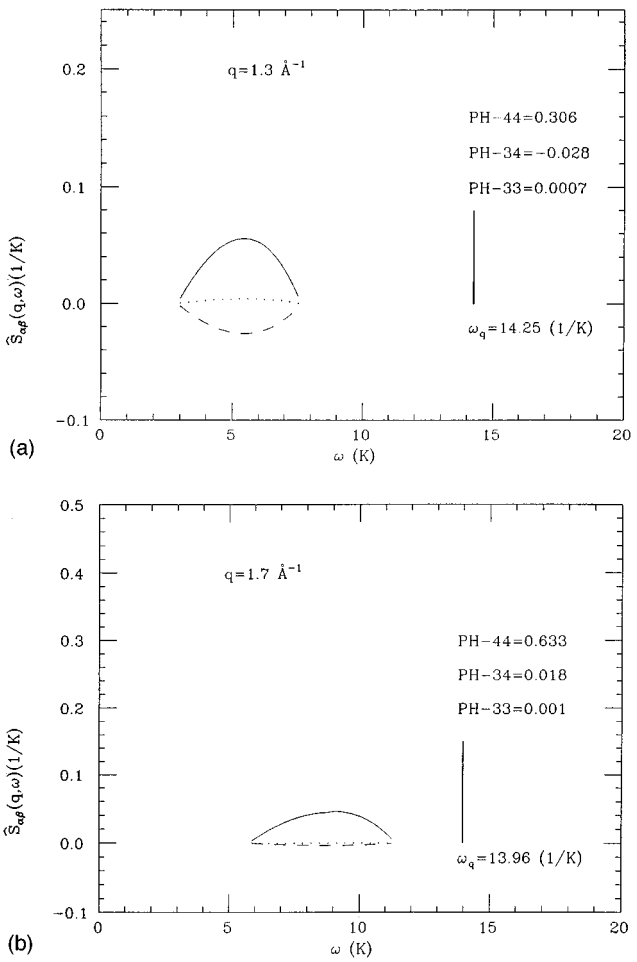

FIG. 6. CBF Partial scattering functions at $q=1.3$ (a) and 1.7 Å^{-1} (b). Continuous line $\hat{S}_{33}$, dashed line $\hat{S}_{34}$ dotted $\hat{S}_{44}$. The PH-$\alpha\beta$ numbers are the strengths of the phonon PSF, located at ω_q.

33 PSF is strongly reduced by the 34 PSF, which practically disappears at $q=1.7$ Å^{-1}. The 44 PSF is always negligible in this sector. In the phonon sector, the 44 PSF is the dominant one. The 33 component always results to be very small. The 34 PSF at $q=1.3$ Å^{-1} slightly reduces the scattering function, while at $q=1.7$ Å^{-1} increases it.

In order to compare with the experimental scattering function, the theoretical PSF's have to be convoluted with the experimental broadening functions. As at these momentum transfers the phonon peak is still δ shaped, because there is no overlap with the multiphonon background, we assume, in accordance with the authors of Ref. 6, that the width in energy of the low temperature results in that reference is entirely due to the instrumental resolution. For this reason we have convoluted the phonon peak with a Gaussian having an average half maximum width of 1.3 K. A Gaussian with a width of 1.2 K (Ref. 37) has been used for the 1p-1h response.

The convoluted total scattering functions are compared with the experimental results of Ref. 6 in Figs. 7(a), 7(b), and 7(c) at $q=1.1$, 1.5, and 1.7 Å^{-1}, respectively, for the 4.7% mixture we have considered so far.

At $q=1.1$ Å^{-1}, both the position and the strength of the phonon branch are well described by our calculation. When

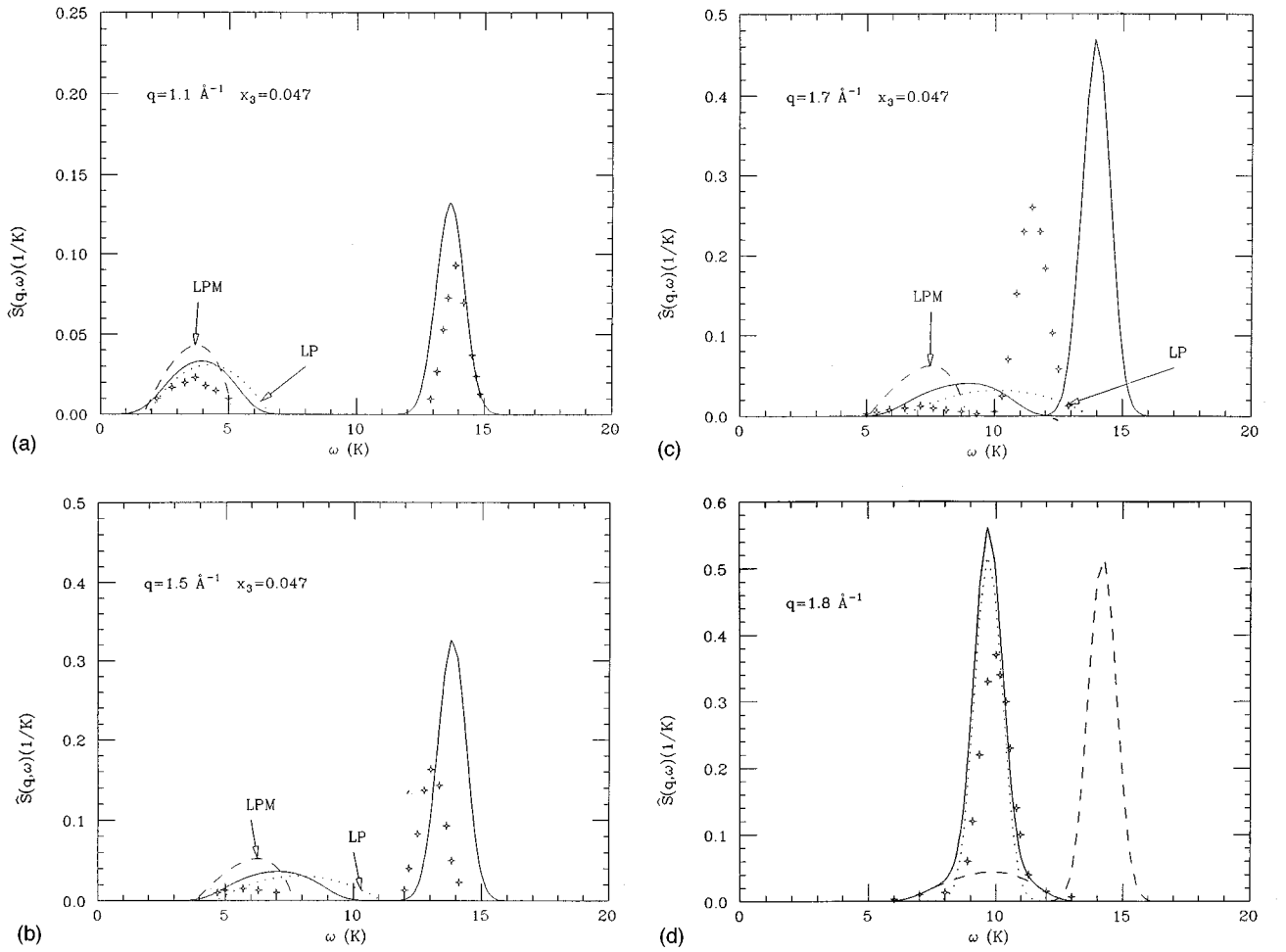

FIG. 7. Total scattering functions at $q=1.1$ (a), $q=1.5$ (b), $q=1.7$ (c) and $q=1.8$ Å^{-1} (d) (solid lines). Also shown (a–c) are the 1p-1h responses with the LP (dotted lines) and LPM (dashed lines) spectra and the experimental data (crosses). In (d), the dashed lines are the 1p-1h and phonon scattering functions and the dotted line is the shifted phonon scattering function (see text).

approaching the roton minimum region, the agreement worsens and we overestimate the experimental data. As discussed previously, we expect that the use of SA will improve the CBF description.

This feature is particularly relevant in the q region where the experimental 1p-1h and phonon branches overlap ($q \geqslant 1.8$ Å^{-1}). Because the CBF ^{4}He excitation spectrum beyond the maxon is higher than the measured one, the computed CBF branches do not overlap, as it is shown in Fig. 7(d) by the dashed curves. We have also shifted the position of the phonon response to its measured peak value of $\omega \sim 10$ K (dotted curve) and added it to the 1p-1h contribution. The result (full curve) is compared with the experiment.[6]

As far as the 1p-1h sector is concerned, the use of the CBF-CA SPE slightly misses the location of the bump, well described in turn by a LPM parametrization, which is essentially a fit to the experimental data. We recall that the relevant difference between the LPM and the CBF-CA energies lies in the γ-parameter value, smaller by a factor ~ 0.4 in the latter case. A simple, quadratic LP parametrization with $m_3^* = 2.3 m_3$ seems to be ruled out. Notice that the 1p-1h branch has been calculated with a nonquadratic SPE, therefore the resulting band is not symmetric and its peak location does not follow a quadratic law.

The ^{3}He scattering function $\hat{S}_3(q,\omega)$, defined as

$$\hat{S}_3(q,\omega) = \frac{x_4\sigma_4 + x_3(\sigma_3^c + \sigma_3^i)}{x_3(\sigma_3^c + \sigma_3^i)} \hat{S}(q,\omega), \tag{58}$$

and the function $\overline{S_3}(q,\omega)$, given by

$$\overline{S_3}(q,\omega) = \frac{\sigma_3 S_{33}(q,\omega) + \sigma_3^i S_{33}^I(q,\omega)}{\sigma_3^c + \sigma_3^i}, \tag{59}$$

in the 1p-1h sector, are given in Fig. 8. The figures contains also the convolution of $\hat{S}_3(q,\omega)$ with the experimental broadening function and the experimental results of Ref. 6, at $q=1.3$ Å^{-1}. $\hat{S}_3$ and S_3 are identical if $S_{34}^{1p-1h} = S_{44}^{1p-1h} = 0$. So, their differences are basically a measure of the importance of the 34 contribution (the 44 one being negligible). Our results show a large suppression of S_{33}^{1p-1h} due to S_{34}^{1p-1h} which brings the CBF response much closer to the experiments.

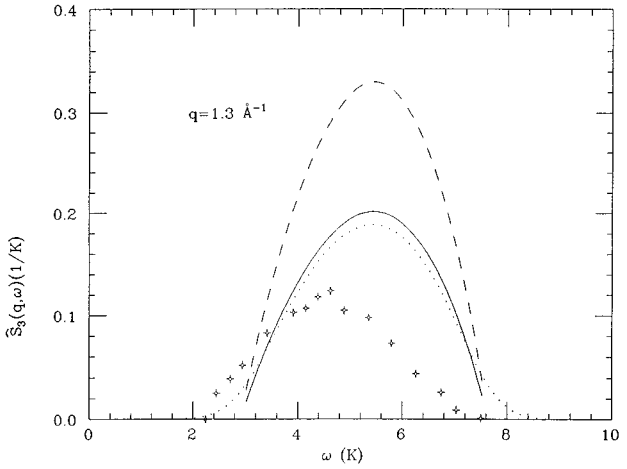

FIG. 8. 1p-1h ^{3}He scattering function at $q=1.3$ Å^{-1}. The solid line is $\hat{S}_3(q,\omega)$, the dashed line is $S_3(q,\omega)$, the dotted line is the experimental convolution of $\hat{S}_3(q,\omega)$ and crosses are the experimental data.

V. CONCLUSIONS

Correlated basis perturbation theory has been used to microscopically compute the scattering function in a $x_3=4.7\%$ ^{3}He-^{4}He mixture at $T=0$. The theory has allowed for explicitly separating the different contributions to the response and for semiquantitatively assessing the relevance of the 34 component. In the 1p-1h region, the S_{33}^{1p-1h} response is sizeably reduced by S_{34}^{1p-1h} up to $q\simeq 1.5$ Å^{-1}, whereas S_{44}^{1p-1h} is always negligible. A similar effect, even if smaller in magnitude, is present in the phonon-roton sector, where the dominant S_{44}^{1PH} is only slightly modified by S_{34}^{1PH}

The responses have been computed by inserting correlated 1p-1h and one- and two-phonon intermediate states. Also the possible decay of one-phonon into two-phonon states has been estimated in boson-boson approximation and using the convolution approximation for the three-body distribution functions.

The microscopic quasiparticle ^{3}He energies clearly show a deviation from the simple LP form. The energies have been actually computed for the single impurity problem, but we do not believe that their evaluation in the low concentration mixture will dramatically change our findings. In particular, a deviation from LP was advocated in Ref. 6 to explain the experimental 1p-1h response, in contrast with a possible large change of the ^{3}He effective mass in mixture (from $m_3^*=2.3m_3$ at $x_3=0$ to $m_3^*=2.9m_3$ at $x_3=4.7\%$). CBF still does not reproduce fully quantitatively the data, and a more accurate calculation is needed.

The ^{4}He excitation spectra in the phonon-roton branch of the pure system and the mixture at SVP have been compared. The shift between the two excitations appears to be due to the change in density. CBF gives a good description of the maxon region, but overestimates the roton, even if it gives an almost correct q value for the change of sign of the shift .

The CBF scattering function at low momenta gives a reasonable description of the scattering data (both for the position and strength). The agreement worsens as q increases. The peaks are located at too a large energy and their strength is overestimated. We believe that the reason of this lies in the approximations made to compute the decay of 1PH states into 2PH and in the lack of higher intermediate states, which become more and more important as the momentum increases. In particular, the 1p-1h sector does not include two probably relevant contributions: the decays of 1p-1h states into (1) 2p-2h and (2) 1PH states. The former adds large energy tails to the 1p-1h bump reducing its strength, and the latter is known to be responsible for a large part of the ^{3}He effective mass. Our CBF calculation includes the real part of the 1p-1h into 1PH decay but does not consider its imaginary part.

The 34 contribution to the total scattering function is especially visible in the ^{3}He scattering function in the 1p-1h region, where its introduction reduces the response by a factor ~ 0.6 at $q=1.3$ Å^{-1}. However, the size of the effect rapidly decreases with q, becoming almost negligible at $q\simeq 2$ Å^{-1}.

In conclusion, we have microscopically established the complex structure of the ^{3}He-^{4}He response using CBF theory. More work is clearly needed in order to give a fully quantitative description of both the excitations and the responses of the Helium mixtures. However, from our results, we believe that CBF is a promising tool in view of achieving this goal.

ACKNOWLEDGMENTS

The authors are grateful to Bjorn Fåk for several fruitful exchanges and acknowledge useful discussions with Jordi Boronat. This research was supported in part by DGICYT (Spain) Grant No. PB92-0761, the agreement CICYT (Spain)–INFN (Italy) and the Acción Integrada program (Spain).

[1] C. Ebner and D.O. Edwards, Phys. Rep. C **2**, 77 (1970).
[2] G. Baym and C. Phetick, in *The Properties of Liquid and Solid Helium*, edited by K.H. Benneman and J.B. Ketterson (Wiley, New York, 1978) Vol. 2.
[3] R. De Bruyn Ouboter and C.N. Yang, Physica B **144**, 127 (1987).
[4] P.A. Hilton, R. Scherm, and W.G. Stirling, J. Low. Temp. Phys. **27**, 851 (1978).
[5] R.N. Bhatt, Phys. Rev. B **18**, 2108 (1978).
[6] B. Fåk, K. Guckelsberger, M. Korfer, R. Scherm, and A.J. Dianoux, Phys. Rev. B **41**, 8732 (1990).
[7] Y. Wang and P.E. Sokol, Phys. Rev. Lett. **72**, 1040 (1994).
[8] A. Szprynger and M. Lucke, Phys. Rev. B **32**, 4442 (1985).
[9] E. Krotscheck and M. Saarela, Phys. Rep. **232**, 1 (1993).
[10] W. Hsu, D. Pines, and C.H. Aldrich, Phys. Rev. B **32**, 7179 (1985).
[11] M. Weyrauch and A. Szprynger, Phys. Rev. B **51**, 12 698 (1995).
[12] J. Boronat, F. Dalfovo, F. Mazzanti, and A. Polls, Phys. Rev. B **48**, 7409 (1993).
[13] J.W. Clark and E. Feenberg, Phys. Rev. **113**, 338 (1959).

[14] Q.N. Usmani, S. Fantoni, and V.R. Pandharipande, Phys. Rev. B **26**, 6123 (1982).
[15] E. Manousakis, S. Fantoni, V.R. Pandharipande, and Q.N. Usmani, Phys. Rev. B **28**, 3770 (1983).
[16] M. Viviani, E. Buendía, S. Fantoni, and S. Rosati, Phys. Rev. B **38**, 4523 (1988).
[17] A. Fabrocini, S. Fantoni, S. Rosati, and A. Polls, Phys. Rev. B **33**, 6057 (1986).
[18] D.S. Greywall, Phys. Rev. B **20**, 2643 (1979).
[19] J.R. Owers-Bradley, P.C. Main, R.M. Browley, G.J. Batey, and R.J. Church, J. Low Temp. Phys. **72**, 201 (1988).
[20] L.D. Landau and I.M. Khalatnikov, Zh. Éksp. Teor. Fiz. **19**, 637 (1948).
[21] E. Feenberg, *Theory of Quantum Fluids* (Academic Press, New York, 1969).
[22] J. Boronat, A. Polls, and A. Fabrocini, J. Low Temp. Phys. **91**, 275 (1993).
[23] A. Fabrocini and S. Fantoni, Nucl. Phys. **A503**, 375 (1989).
[24] A. Fabrocini, Phys. Lett. B **322**, 171 (1994).
[25] O. Benhar, A. Fabrocini, S. Fantoni, and I. Sick, Nucl. Phys. **A579**, 493 (1994).
[26] E. Manousakis and V.R. Pandharipande, Phys. Rev. B **33**, 150 (1986).
[27] V.F. Sears, in *Neutron Scattering*, Vol. 23A of *Methods of Experimental Physics*, edited by K. Skold and D.L. Price (Academic, New York, 1986).
[28] R.P. Feynman, Phys. Rev. **94**, 262 (1954)
[29] J.C. Owen, Phys. Rev. B **23**, 5815 (1981).
[30] A. Fabrocini and A. Polls, Phys. Rev. B **30**, 1200 (1984).
[31] T. Chakraborty, A. Kallio, L.J. Lannto, and P. Pietilainen, Phys. Rev. **B27**, 3061 (1983).
[32] M.D. Miller, Ann. Phys. **127**, 367 (1980).
[33] R.A. Cowley and A.D.B. Woods, Can. J. Phys. **49**, 177 (1971).
[34] D.K. Lee and F.J. Lee, Phys. Rev. B **11**, 4318 (1975).
[35] B. Friedman and V.R. Pandharipande, Phys. Lett. **100B**, 205 (1981).
[36] A. Fabrocini, L. Vichi, F. Mazzanti, and A. Polls (unpublished).
[37] B. Fåk (private communication).